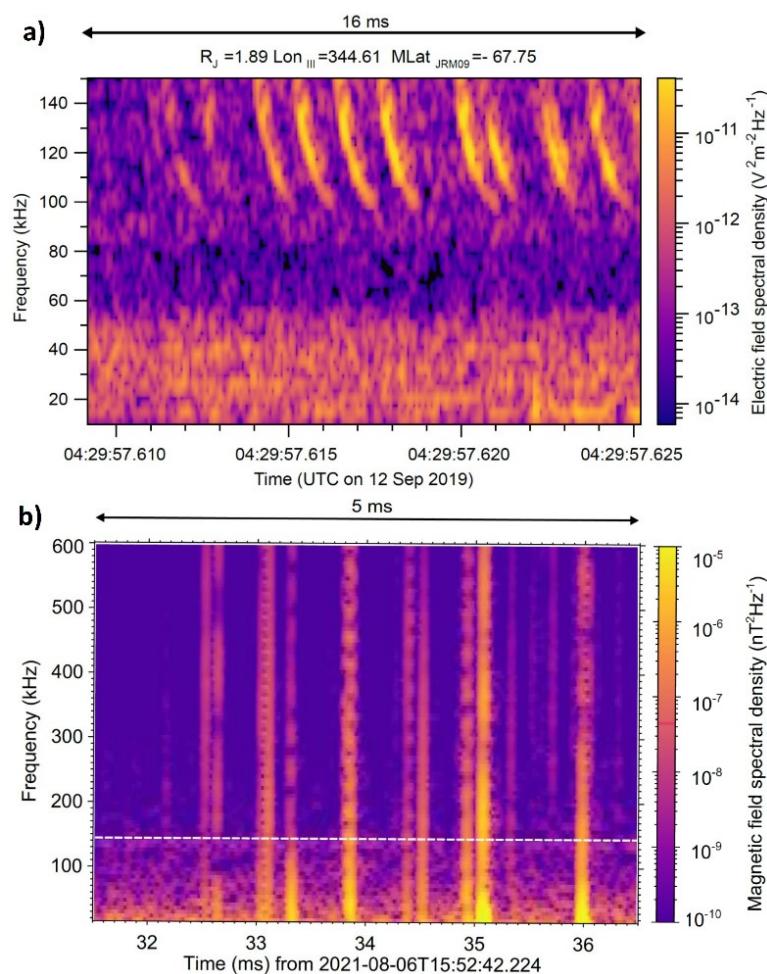


Results of the Department of Space Physics, Institute of Atmospheric Physics, Czech Academy of Sciences, published in 2023

1. Lightning at Jupiter pulsates with a similar rhythm as in-cloud lightning at Earth

Our knowledge about the fine structure of lightning processes at Jupiter was substantially limited by the time resolution of previous measurements. Recent observations of the Juno mission revealed electromagnetic signals of Jovian rapid whistlers at a cadence of a few lightning discharges per second, comparable to observations of return strokes at Earth. The duration of these discharges was below a few milliseconds and below one millisecond in the case of Jovian dispersed pulses, which were also discovered by Juno. However, it was still uncertain if Jovian lightning processes have the fine structure of steps corresponding to phenomena known from thunderstorms at Earth. We therefore analyzed results collected by the Juno Waves instrument during 5 years of measurements at 125-microsecond resolution. We identified radio pulses with typical time separations of one millisecond, which suggested step-like extensions of lightning channels and indicated that Jovian lightning initiation processes were similar to the initiation of intracloud lightning at Earth.



a) Frequency-time spectrogram of power spectral density of electric field fluctuations of a group of dispersed pulses recorded by the Juno satellite on 12 September 2017 after 04:29:57 UTC at a radial

distance of 1.89 RJ (Jovian radii). b) Frequency-time spectrogram of power spectral density of magnetic field fluctuations showing the 5 ms long detail of the initiation of an intracloud flash that occurred on 6 August 2021 at 15:52:42 UTC. The measurement was conducted by a broadband magnetic field antenna (5 kHz to 90 MHz) installed at the Dlouhá Louka observatory in Czechia. For comparison with the dispersed pulses from panel a), the white dashed line indicates the upper frequency limit of the Juno measurements.

Reference:

I. Kolmašová, O. Santolík, M. Imai, W. S. Kurth, G. B. Hospodarsky, J. E. P. Connerney, S. J. Bolton, R. Lán (2023). Lightning at Jupiter pulsates with a similar rhythm as in-cloud lightning at Earth. *Nature communications* 14, 207. Doi:10.1038/s41467-023-38351-6.

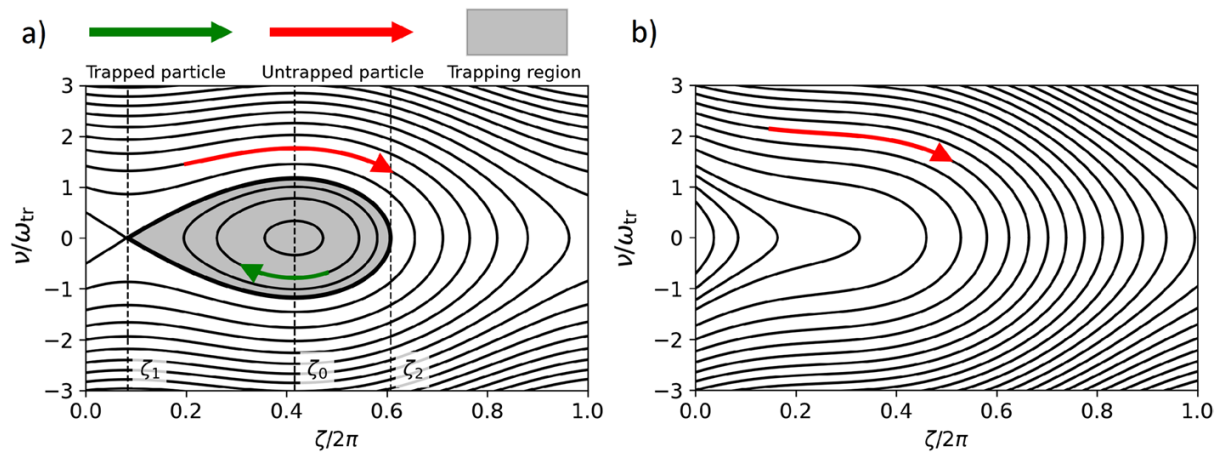
Related references:

Nature Research Highlights: Jupiter's lightning has rhythm — just like Earth's, 23 May 2023. Doi: 10.1038/d41586-023-01698-3.

Kurth, W. S., Wilkinson, D. R., Hospodarsky, G. B., Santolík, O., Averkamp, T. F., Sulaiman, A. H., et al. (2023). Juno plasma wave observations at Europa. *Geophysical Research Letters*, 50, e2023GL105775. Doi:10.1029/2023GL105775.

2. Theories of Growth and Propagation of Parallel Whistler-Mode Chorus Emissions: A Review

The significant role of nonlinear wave–particle interactions in the macrodynamics and microdynamics of the Earth's outer radiation belt has long been recognized. Electron dropouts during magnetic storms, microbursts in atmospheric electron precipitation, and pulsating auroras are all associated with the rapid scattering of energetic electrons by the whistler-mode chorus, a structured electromagnetic emission known to reach amplitudes of about 1% of the ambient magnetic field. Despite the decades of experimental and theoretical investigations of chorus and the recent progress achieved through numerical simulations, there is no definitive theory of the chorus formation mechanism, not even in the simple case of parallel (one-dimensional) propagation. We followed the evolution of these theories from their beginnings in the 1960s to the current state, including newly emerging self-consistent excitation models. A critical review of the unique features of each approach was provided, taking into account the most recent spacecraft observations of the fine structure of chorus. Conflicting interpretations of the role of resonant electron current and magnetic field inhomogeneity are discussed. We also discussed the interplay between nonlinear growth and microscale propagation effects and identify future theoretical and observational challenges stemming from the two-dimensional aspects of chorus propagation.



Phase portrait showing the behaviour of electrons near cyclotron resonance with a constant inhomogeneity factor $S = -0.5$ (panel a) and $S = -1.2$ (panel b). Particles in the trapping region (green arrow) oscillate around a constant phase ζ_0 with respect to the circularly polarized electromagnetic field of chorus waves. Untrapped particles (red arrow) are not phase-locked.

Reference:

Hanzelka, M. and **Santolík, O.** (2023). Theories of Growth and Propagation of Parallel Whistler-Mode Chorus Emissions: A Review, *Surveys in Geophysics*, Doi: 10.1007/s10712-023-09792-x.

Related references:

Hartley, D. P., Christopher, I. W., Kletzing, C. A., Kurth, W. S., **Santolík, O.**, **Kolmašová, I.**, et al. (2023). Chorus wave properties from Van Allen Probes: Quantifying the impact of the sheath corrected electric field. *Geophysical Research Letters*, 50. Doi:10.1029/2023GL102922.

Kletzing, C. A., Bortnik, J., Hospodarsky, G., Kurth, W. S., **Santolík, O.**, Smith, C.W., Christopher, I. W., Hartley, D. P., **Kolmašová, I.**, Sen Gupta, A. (2023). The Electric and Magnetic Fields Instrument Suite and Integrated Science (EMFISIS): Science, Data, and Usage Best Practices, *Space Science Reviews*, 219, 28. Doi: 10.1007/s11214-023-00973-z.

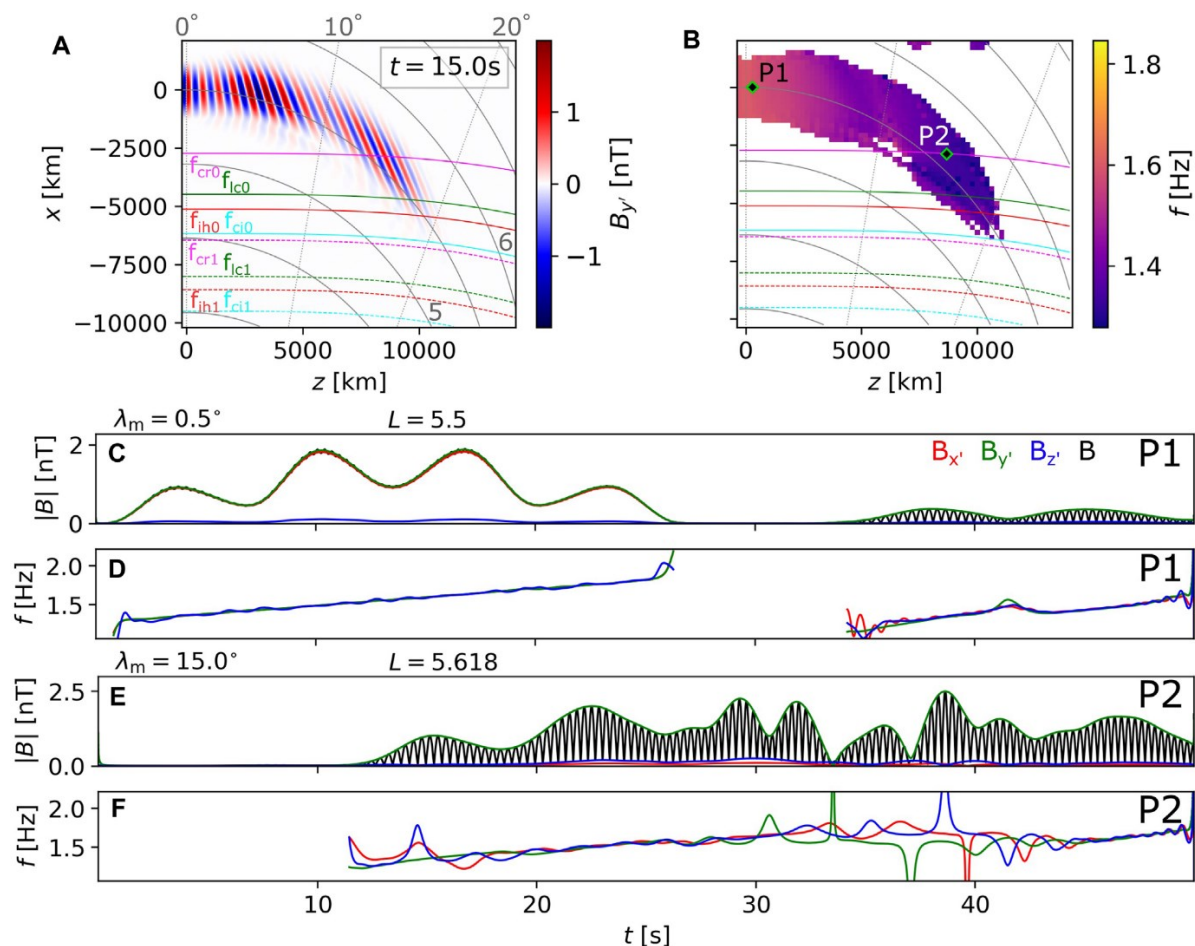
Huang, S., Li, W., Ma, Q., Shen, X.-C., Capannolo, L., **Hanzelka, M.**, Chu, X., Ma, D., Bortnik, J., and Wing, S. (2023). Deep learning model of hiss waves in the plasmasphere and plumes and their effects on radiation belt electrons. *Front. Astron. Space Sci.* 10:1231578. Doi: 10.3389/fspas.2023.1231578.

Bezděková, B., Němec, F., Manninen, J., **Santolík, O.**, Hospodarsky, G. B., and Kurth, W. S. (2023), Very low frequency whistler mode wave events observed simultaneously by the Kannuslehto station and Van Allen Probes, *J. Geophys. Res. Space Phys.*, 128(1), e2022JA03107, doi: 10.1029/2022JA031078.

Brunet, A., Dahmen, N., Katsavrias, C., **Santolík, O.**, et al., 2023: Improving the Electron Radiation Belt Nowcast and Forecast Using the SafeSpace Data Assimilation Modeling Pipeline, *Space Weather*, 21, 8, e2022SW003377. Doi:10.1029/2022SW003377.

3. Full-wave modeling of EMIC wave packets: ducted propagation and reflected waves

Electromagnetic ion cyclotron (EMIC) waves can scatter radiation belt electrons with energies of a few hundred keV and higher. To accurately predict this scattering and the resulting precipitation of these relativistic electrons on short time scales, we need detailed knowledge of the wave field's spatio-temporal evolution, which cannot be obtained from single spacecraft measurements. Our study presented EMIC wave models obtained from two-dimensional (2D) finite-difference time-domain (FDTD) simulations in the Earth's dipole magnetic field. We studied cases of hydrogen band and helium band wave propagation, rising-tone emissions, packets with amplitude modulations, and ducted waves. We analyzed the wave propagation properties in the time domain, enabling comparison with in situ observations. We showed that cold plasma density gradients can keep the wave vector quasiparallel, guide the wave energy efficiently, and have a profound effect on mode conversion and reflections. The wave normal angle of unducted waves increases rapidly with latitude, resulting in reflection on the ion hybrid frequency, which prohibits propagation to low altitudes. The modeled wave fields can serve as an input for test-particle analysis of scattering and precipitation of relativistic electrons and energetic ions.



Field components and propagation properties of waves from simulation run with input parameter Set 4 (rising-tone unducted hydrogen band wave packet with four subpackets). (A) Magnetic field component $B_{x'}$ perpendicular to the local field line (perpendicular to the meridional plane). Snapshot taken at $t = 15$ s. Crossings of characteristic frequencies for wave at frequency ω_0 are represented by solid lines as before, and the crossing for the final frequency ω_1 are plotted with dashed lines. (B) Instantaneous wave frequency snapshot, obtained as a power-weighted average of frequencies of

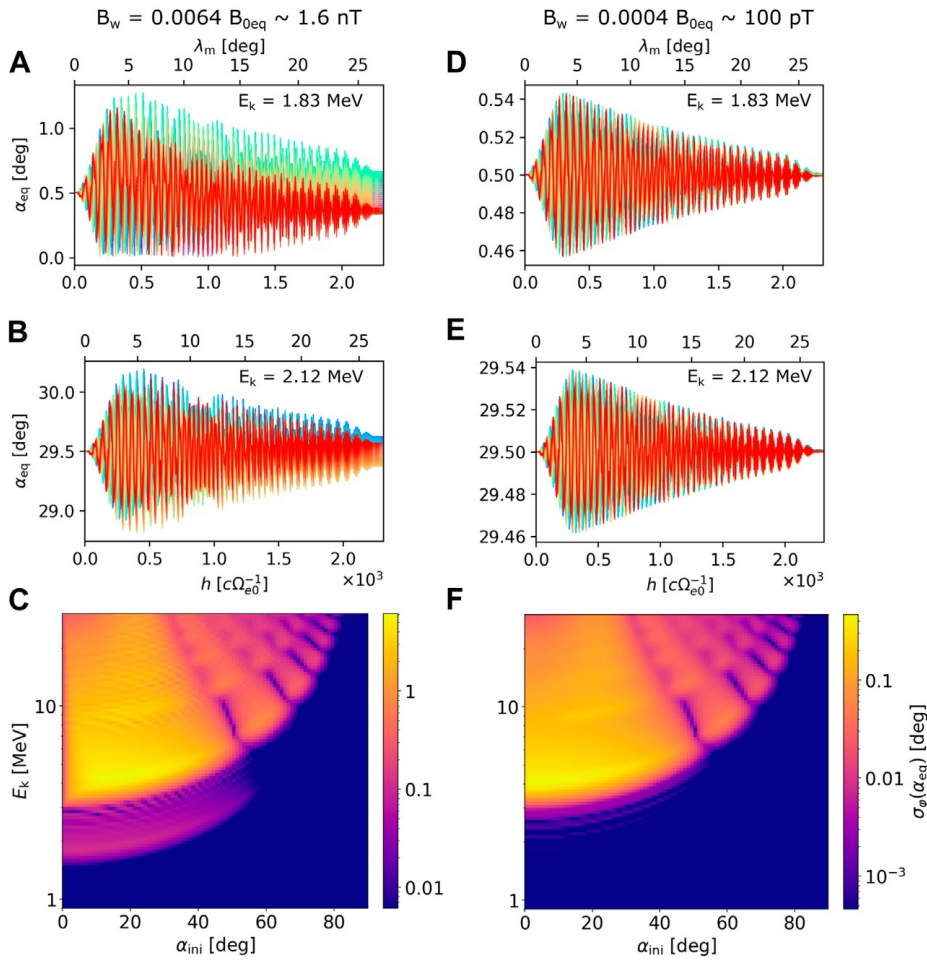
the three magnetic components. Labels P1 and P2 show positions of probes that collected data analyzed in the following panels. (C) Probe P1 measured amplitude envelopes of the magnetic field components B_x' , B_y' , and B_z' plotted in red, green, and blue, respectively. The total magnetic field $|B|$ is plotted with a black line. (D) Instantaneous frequencies from Probe P1, color coded as in the previous panel. (E, F) Same as panels (C, D), but with data from probe P2.

Reference:

Hanzelka, M., Li, W., Ma, Q., Qin, M., Shen, X.-C., Capannolo, L., and Gan, L. (2023), Full-wave modeling of EMIC wave packets: ducted propagation and reflected waves. *Front. Astron. Space Sci.* 10:1251563. Doi: 10.3389/fspas.2023.1251563.

4. Parametric analysis of pitch angle scattering and losses of relativistic electrons by oblique EMIC waves

We analyzed the effects of electromagnetic ion cyclotron (EMIC) waves on relativistic electron scattering and losses in the Earth's outer radiation belt. EMIC emissions are commonly observed in the inner magnetosphere and are known to reach high amplitudes, causing significant pitch angle changes in primarily >1 MeV electrons via cyclotron resonance interactions. We run test-particle simulations of electrons streaming through helium band waves with different amplitudes and wave normal angles and assessed the sensitivity of advective and diffusive scattering behaviors to these two parameters, including the possibility of very oblique propagation. The numerical analysis confirmed the importance of harmonic resonances for oblique waves, and the very oblique waves are observed to efficiently scatter both co-streaming and counter-streaming electrons. However, strong finite Larmor radius effects limit the scattering efficiency at high pitch angles. Recently discussed force-bunching effects and associated strong positive advection at low pitch angles are, surprisingly, shown to cause no decrease in the phase space density of precipitating electrons, and we demonstrated that the transport of electrons into the loss cone balances out the scattering out of the loss cone. In the case of high-amplitude obliquely propagating waves, weak but non-negligible losses were detected well below the minimum resonance energy, and we identified them as the result of non-linear fractional resonances. Simulations and theoretical analysis suggested that these resonances might contribute to subrelativistic electron precipitation but are likely to be overshadowed by non-resonant effects.



Behavior of fractional resonances explained by particle trajectories and standard deviations in equatorial pitch angle for an EMIC wave with wave normal angle $\vartheta_k = 70^\circ$ with respect to the background magnetic field (A–B) Changes in pitch angle along the field line at energies well below the equatorial fundamental resonance energy $E_{Rmin} \approx 4$ MeV. The wave amplitude is $B_{w0} = 1.6$ nT. (C) Standard deviation in equatorial pitch angle plotted in logarithmic scale that spans three orders of magnitude. Weak resonant effects near 2 MeV become apparent. (D–F) Same as (A–C), but for a 16 times smaller wave amplitude. The resonant effects near $E_{Rmin}/2$ are now insubstantial compared to the fundamental resonance.

Reference:

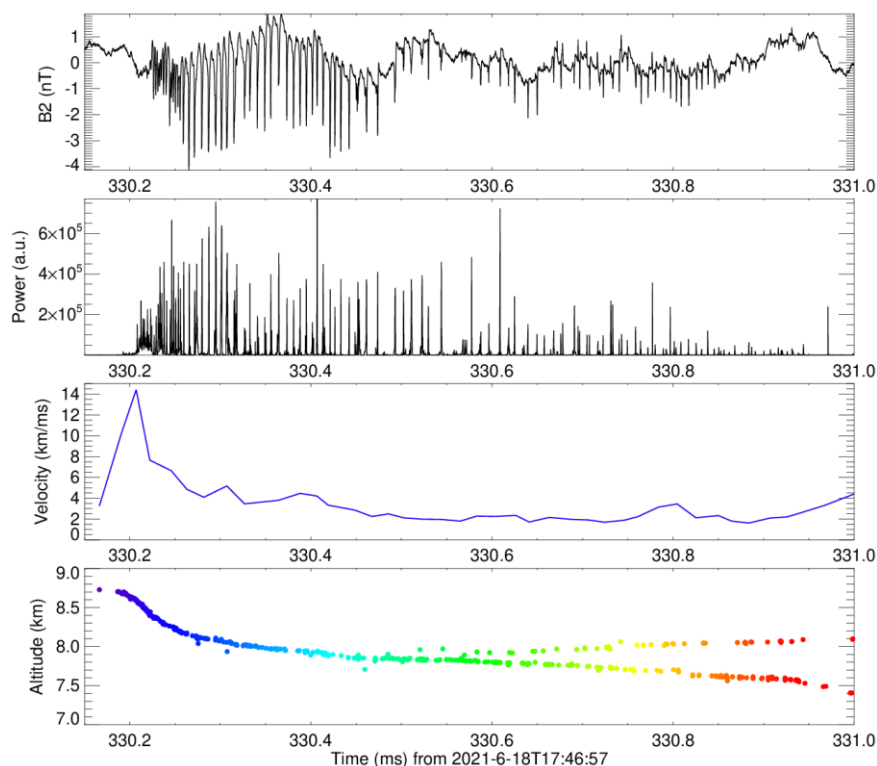
Hanzelka, M., Li, W. and Ma, Q. (2023), Parametric analysis of pitch angle scattering and losses of relativistic electrons by oblique EMIC waves. *Front. Astron. Space Sci.* 10:1163515. Doi: 10.3389/fspas.2023.1163515.

Related reference:

Capannolo, L., Li, W., Ma, Q., Qin, M., Shen, X.-C., Angelopoulos, V., **Hanzelka, M.** et al. (2023). Electron precipitation observed by ELFIN using proton precipitation as a proxy for electromagnetic ion cyclotron (EMIC) waves. *Geophysical Research Letters*, 50. Doi:10.1029/2023GL103519.

5. A Strong Pulsing Nature of Negative Intracloud Dart Leaders Accompanied by Regular Trains of Microsecond-Scale Pulses

We reported the first observations of negative intracloud (IC) dart-stepped leaders accompanied by regular trains of microsecond-scale pulses, simultaneously detected by our shielded broadband magnetic loop antennas and the radio telescope Low Frequency Array (LOFAR). Four investigated pulse trains occurred during complicated IC flashes on 18 June 2021, when heavy thunderstorms hit the Netherlands. The pulses within the trains were unipolar, a few microseconds wide, and with an average inter-pulse interval of 5–7 μ s. The broadband pulses perfectly matched energetic, regularly distributed, and relatively isolated bursts of very high frequency sources localized by LOFAR. All trains were generated by negative dart-stepped leaders propagating at a lower speed than usual dart leaders. They followed channels of previous leaders occurring within the same flash several tens of milliseconds before the reported observations. The physical mechanism remains unclear as to why we observed dart-stepped leaders, which showed mostly regular stepping, emitting energetic microsecond-scale pulses.



Event C1: (a) Magnetic field pulse train measured by the Shielded Loop Antenna with a Versatile Integrated Amplifier (SLAVIA) antenna on 18 June 2021. (b) Very High Frequency (VHF) power detected at the same time by the Low Frequency Array (LOFAR) antenna CS002. (c) Average velocity of the leader movement. (d) Sources of VHF radiation located by the LOFAR impulsive imager.

Reference:

Kolmašová, I., Scholten, O., **Santolík, O.,** Hare, B. M., Zacharov, P., **Lán, R.,** et al. (2023). A strong pulsing nature of negative intracloud dart leaders accompanied by regular trains of microsecond-scale pulses. *Geophysical Research Letters*, 50. Doi:10.1029/2023GL103864.

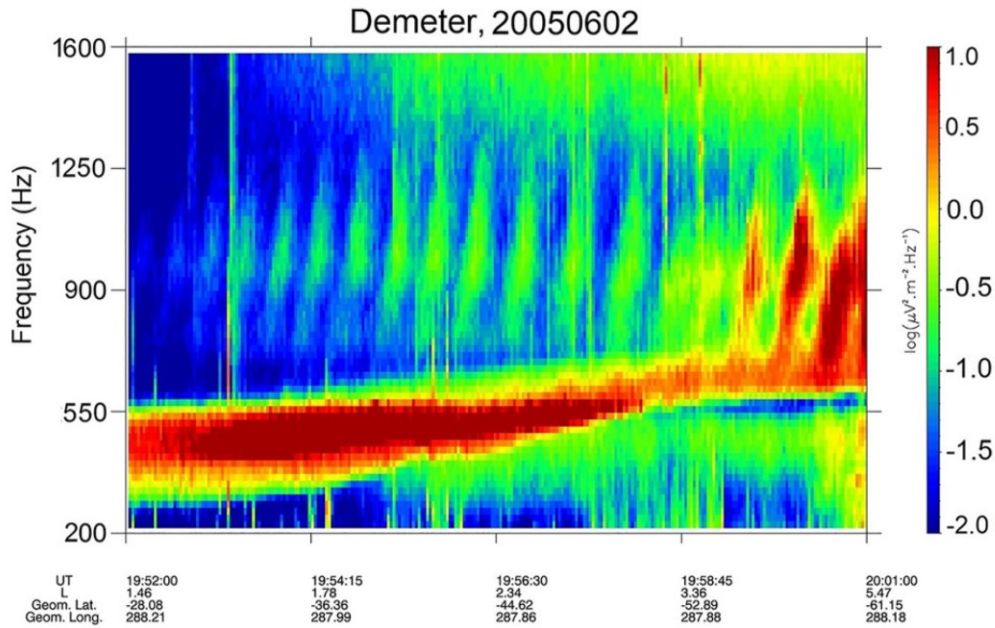
Related references:

Tomicic, M., Chanrion, O., Farges, T., Mlynarczyk, J., **Kolmašová, I.**, Soula, S., et al. (2023). Observations of elves and radio wave perturbations by intense lightning. *Journal of Geophysical Research: Atmospheres*, 128. Doi:10.1029/2022JD036541.

Bandara, S., Marshall, T., and Stolzenburg, M. (2023), Further studies of positive Narrow Bipolar Events detected at close range, *Atmospheric Research* 286, 106668. Doi:10.1016/j.atmosres.2023.106668.

6. Quasiperiodic ELF/VLF emissions associated with corresponding pulsations of the geomagnetic field

We presented a comparison between properties of quasiperiodic (QP) extra low frequency/very low frequency emissions observed by the low-altitude DEMETER spacecraft and ultra-low frequency (ULF) geomagnetic field pulsations measured on the ground by the Canadian Array for Realtime Investigations of Magnetic Activity system of flux-gate magnetometers and by the Sodankylä Geophysical Observatory magnetometer. Altogether, we have analyzed 398 QP events observed at the times when DEMETER was close to the ground-based magnetometers. The modulation periods of the analyzed QP events were larger than 10 s and their frequency bandwidths were larger than 200 Hz. For a part of QP emissions with modulation periods about 30 s, there was a good agreement between the modulation periods and peak frequencies of ULF magnetic field pulsations measured on the ground. These QP emissions appeared to be closely associated with coincident geomagnetic pulsations (QP1 type), and they represented ~18% of the total number of analyzed QP events. No corresponding geomagnetic pulsations were identified in the remaining 82% of QP events (QP2type). The intensity of QP1 events did not seem to correlate with the intensity of geomagnetic field pulsations, while the intensity of QP2 events increased with the integral intensity of geomagnetic field pulsations. Based on the observed association between QP emissions and geomagnetic field pulsations, we estimated the radial distance of the generation region of QP1 emissions to $L \sim 7$.



Frequency-time spectrograms of power spectral density of electric field fluctuations corresponding to a quasiperiodic (QP) event measured on 2 June 2005 between 19.52 UT and 20:02 UT in the Southern hemisphere. A set of individual QP elements slowly fading out toward lower geomagnetic latitudes can be seen at frequencies between ~ 700 and ~ 1700 Hz.

Reference:

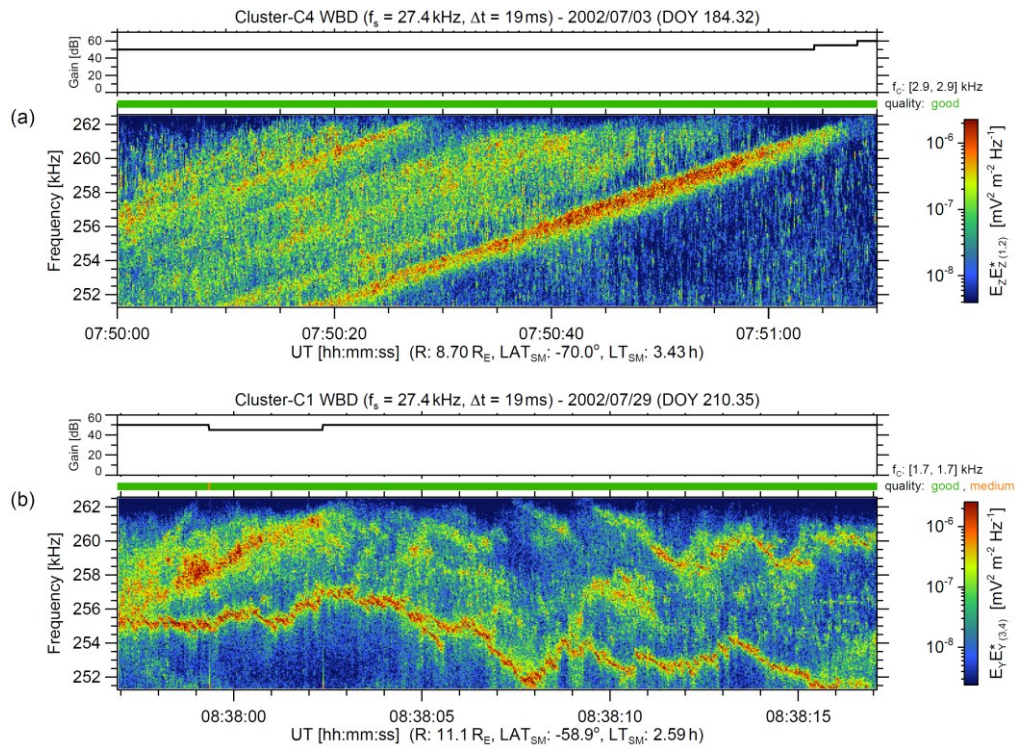
Hajoš, M., Němec, F., Demekhov, A., Santolík, O., Parrot, M., Raita, T., Bezděková, B. (2023), Quasiperiodic ELF/VLF emissions associated with corresponding pulsations of the geomagnetic field, *J. Geophys. Res. Space Phys.*, 128(4), e2022JA031110. Doi:10.1029/2022JA031103.

Related reference:

Němec, F., Manninen, J., Santolík, O., Hospodarsky, G. B., & Kurth, W. S. (2023). Magnetospheric line radiation observed close to the source: Properties and propagation. *J. Geophys. Res. Space Phys.*, 128. Doi:10.1029/2023JA031454.

7. Classification of the spectral fine structure in auroral kilometric radiation

Auroral Kilometric Radiation (AKR) is generated by unstable energetic electron populations in the auroral region of Earth's magnetosphere. A mechanism known as the cyclotron maser instability amplifies weak background radiation at the expense of particle energy. However, this instability alone cannot explain frequent observations of AKR spectral fine structures when recorded with sufficiently high time and frequency resolution. We analyzed observations of AKR from the Cluster Wideband Receiver and gave an overview of the different types of spectral fine structures found in this dataset in years 2002 and 2003. A classification scheme was introduced, and the occurrence rate for each class of fine structure was investigated in a statistical analysis. Possible generation mechanisms was discussed in relation to the observations.



(a) AKR Bands with a positive drift rate (~ 0.22 kHz/s; ~ 80 seconds displayed) and (b) irregularly drifting AKR Snakes (~ 20 seconds displayed). The emission in (a) below the intensive bottom Band is AKR Rain (unresolved).

Reference:

Taubenschuss, U., Fischer, G., Píša, D., Santolík, O., Souček, J. (2023). Classification of the spectral fine structure in auroral kilometric radiation, *C. K. Louis, C. M. Jackman, G. Fischer, A. H. Sulaiman, P. Zucca, Dublin Institute for Advanced Studies (Eds.), Planetary, Solar and Heliospheric Radio Emissions IX*. Doi:10.25546/103089.

Related references:

Fischer, G., **Taubenschuss, U., Píša, D.**, Lamy, L., Wu, S., Ye, S.-Y., Jackman, C. M., O'Dwyer, E. (2023). A particular form of Saturn kilometric radiation at the low end of its spectrum., *C. K. Louis, C. M. Jackman, G. Fischer, A. H. Sulaiman, P. Zucca, Dublin Institute for Advanced Studies (Eds.), Planetary, Solar and Heliospheric Radio Emissions IX*. Doi:10.25546/103099.

Lamy, L., Prangé, P., Morooka, M., Kurth, W. S., **Taubenschuss, U.** (2023), The peak frequency source of Saturn's kilometric radiation., *C. K. Louis, C. M. Jackman, G. Fischer, A. H. Sulaiman, P. Zucca, Dublin Institute for Advanced Studies (Eds.), Planetary, Solar and Heliospheric Radio Emissions IX*. Doi:10.25546/103102.

8. Langmuir waves associated with magnetic holes in the solar wind

Langmuir waves (electrostatic waves near the electron plasma frequency) are often observed in the solar wind and may play a role in the energy dissipation of electrons. The largest amplitude Langmuir waves are typically associated with type II and III solar radio bursts and planetary foreshocks. In

addition, Langmuir waves not related to radio bursts occur in the solar wind, but their source is not well understood. Langmuir waves are observed inside isolated magnetic holes, suggesting that magnetic holes play an important role in the generation of Langmuir waves. We participated in a study of statistical distribution of Langmuir waves in the solar wind at different heliocentric distances. We investigated the relationship between magnetic holes and Langmuir waves. We identified possible source regions of Langmuir waves in the solar wind, other than radio bursts, by analyzing the local plasma conditions. We analyzed data from Solar Orbiter's Radio and Plasma Waves (RPW) and Magnetometer (MAG) instruments. We used the triggered electric field snapshots and onboard statistical data (STAT) of the Time Domain Sampler (TDS) of RPW to identify Langmuir waves and investigate their properties. The plasma densities were derived from the spacecraft potential estimated by RPW. The MAG data were used to monitor the background magnetic field and detect magnetic holes, which are defined as regions with an isolated decrease of 50% or more compared to the background level. The statistical analysis was performed on data from 2020 to 2021, comprising heliocentric distances between 0.5AU and 1AU. We showed that 78% of the Langmuir waves in the solar wind not connected to radio bursts occurred in regions of local magnetic field depletions, including the regions classified as isolated magnetic holes. We also showed that the Langmuir waves occurred more frequently inside magnetic holes than in any other region in the solar wind, which indicates that magnetic holes are important source regions of solar wind Langmuir waves. We found that Langmuir waves associated with magnetic holes in the solar wind typically have lower amplitudes than those associated with radio bursts.

Reference:

Boldú, J. J., Graham, D. B., Morooka, M., André, M., Khotyaintsev, Yu. V., Karlsson, T., **Souček, J., Píša, D.**, and Maksimovic, M. (2023). Langmuir waves associated with magnetic holes in the solar wind, *A&A* 674, A220. Doi:10.1051/0004-6361/202346100.

Related references:

Krasnoselskikh, V. Tsurutani, B. T., Dudok de Wit, T., Walker, S., Balikhin, M., Balat-Pichelin, M..... **Souček, J.** et al. (2023). ICARUS: in-situ studies of the solar corona beyond Parker Solar Probe and Solar Orbiter, *Experimental Astronomy*, 54:277–315. Doi: 10.1007/s10686-022-09878-1.

Kvammen, A., Wickstrøm, K., Kociscak, S., Vaverka, J., Nouzak, L., Zaslavsky, A., Rackovic Babic, K., Gjelsvik, A., **Píša, D., Souček, J.**, and Mann, I. (2023). Machine learning detection of dust impact signals observed by the Solar Orbiter, *Ann. Geophys.*, 41, 69–86. Doi:10.5194/angeo-41-69-2023.

9. Development of scientific spacecraft instrumentation

We have continued our involvement in the development of new scientific spacecraft instrumentation. We have also worked on calibration and operations of spacecraft instruments and subsystems built by our team in the past. This includes operations of the Radio and Plasma Waves instrument on the ESA's Solar Orbiter spacecraft, in-flight calibration, software development, and mission planning for the Radio and Plasma Waves Investigation instrument on the ESA's JUICE spacecraft, development of instruments for the ESA's Comet Interceptor, Vigil, LISA, and Athena spacecraft projects, and in preparation of future lunar missions.

References:

Fletcher, L. N., Cavalié, T., Grassi, D., (...), **Santolík, O., Kolmašová, I.**, et al. (2023). Jupiter Science Enabled by ESA's Jupiter Icy Moons Explorer, *Space Science Reviews*, 219, 7, 53.

Barret, D., Albouys, V., den Herder, J.-W., Massimo Cappi, L. P. Huovelin, J. **Souček, J.**.... et al. (2023). The Athena X-ray Integral Field Unit: a consolidated design for the system requirement review of the preliminary definition phase, *Experimental Astronomy* 55:373–426. Doi:10.1007/s10686-022-09880-7.

Dandouras, I., Taylor, M. G. G. T., De Keyser, J., **Grison, B.**, (...), Štverák, Š., et al. (2023). Space plasma physics science opportunities for the lunar orbital platform - Gateway, *Frontiers in Astronomy and Space Sciences*, 10, 1120302. Doi: 10.3389/fspas.2023.1120302.

Department of Space Physics, Institute of Atmospheric Physics of the Czech Academy of Sciences in 2023

1. Samuel Amrich, student, 20% FTE, till 31 May 2023
2. Radka Balková, secretary, 50% FTE
3. Tomáš Formánek, student, 20% FTE
4. Benjamin Grison, research scientist
5. Michajlo Hajoš, research scientist
6. Miroslav Hanzelka, postdoctoral associate, on leave at Boston University and GFZ Potsdam
7. Pavel Houfek, research engineer, from 1 September 2023
8. Jiří Jánský, research engineer
9. Michaela Jírová, PhD student, 40% FTE
10. Petr Kašpar, research scientist
11. Andrea Kolínská, PhD student, 70% FTE
12. Ivana Kolmašová, senior research scientist
13. *Vratislav Krupař, research scientist, on leave*
14. *Oksana Krupařová, research scientist, on leave*
15. Radek Lán, research engineer
16. Ján Mičko, PhD student, 70% FTE
17. David Píša, research scientist
18. Martin Popek, TLE observer, 25% FTE
19. Kateřina Rosická, student, 20% FTE
20. Ondřej Santolík, senior research scientist, head of the department
21. Jan Snížek, research engineer, 50% FTE
22. Jan Souček, senior research scientist, deputy head of the department
23. *Hana Špačková, on leave*
24. Ulrich Taubenschuss, research scientist
25. Marie Turčičová, postdoctoral associate, 20% FTE, till 31 July 2023
26. Luděk Uhlíř, research engineer